Section 2

Data sets, diagnostic and dynamical investigations, statistical post-processing , multi-year reanalyses and associated studies

Indian Ocean influences on Cold Events over southern Australia

Linden Claire Ashcroft, Ian Simmonds and Alexandre Bernardes Pezza

School of Earth Sciences, The University of Melbourne, Victoria, 3010, Australia
simmonds@unimelb.edu.au

We are exploring the largescale influences on southern Australian 'Cold Events' (CEs), particularly those associated with conditions over the 'upstream' Indian Ocean. We define CEs as the bottom 0.4% of maximum temperatures in Melbourne and in Perth for each calendar month (Perrin and Simmonds 1995, Simmonds and Richter 2000) for the 1958-2006 period. Almost invariably these CEs are associated with an intensive high pressure-low pressure couplet, which is related with the intense cold southerlies. Our previous and current research (Simmonds and Rashid 2001, Ashcroft et al. 2009) has indicated that in southern Australian CEs the anticyclone component of the couplet is usually very long-lived, and can originate weeks before in the west Indian Ocean or even in the Atlantic Ocean.

We here focus on the composite of the SST anomalies in the week leading up to Melbourne summer (December - February) CEs. Figure 1(a) shows that the SST over those seven days are significantly less than normal over broad stretches of the Indian Ocean and the Great Australian Bight. These are the regions over which the high pressure component of the H-L couplet would have passed. The strength and scale of the anomalies is impressive. It can be argued that the presence of these cooler temperatures serve to, in a climatological sense, encourage and intensify high pressure systems passing over them. Consistent with this picture is the fact that positive SST anomalies are found to the south and east of the Tasman Sea, the region over which most of the low pressure components of the couplet form.

A similar display is presented in Fig. 1(b) for the case of Perth winter CEs. The broad structure of the SST anomaly field is very similar, after one takes in account the more westward position of Perth compared to Melbourne.

It is becoming well known how and why the Indian Ocean strongly influences Australian rainfall (Simmonds and Rocha 1991, England et al. 2006). The present work serves to emphasise the important role that the Indian Ocean plays in a wide variety of aspects of Australian weather and climate.

Ashcroft, L. C., A. B. Pezza and I. Simmonds, 2009: Cold events over southern Australia: Synoptic climatology and hemispheric structure. *J. Climate*, **22**, 6679-6698.

England, M. H., C. C. Ummenhofer and A. Santoso, 2006: Interannual rainfall extremes over southwest Western Australia linked to Indian Ocean climate variability. *J. Climate*, **19**, 1948-1969.

Perrin, G., and I. Simmonds, 1995: The origin and characteristics of cold air outbreaks over Melbourne. *Aust. Meteor. Mag.*, **44**, 41-59.

Simmonds, I., and H. A. Rashid, 2001: An investigation of a dramatic cold outbreak over southeast Australia. *Aust. Meteor. Mag.*, **50**, 249-261.

Simmonds, I., and T. Richter, 2000: Synoptic comparison of cold events in winter and summer in Melbourne and Perth. *Theor. Appl. Climatol.*, **67**, 19-32.

Simmonds, I., and A. Rocha, 1991: The association of Australian winter climate with ocean temperatures to the west. *J. Climate*, **4**, 1147-1161.

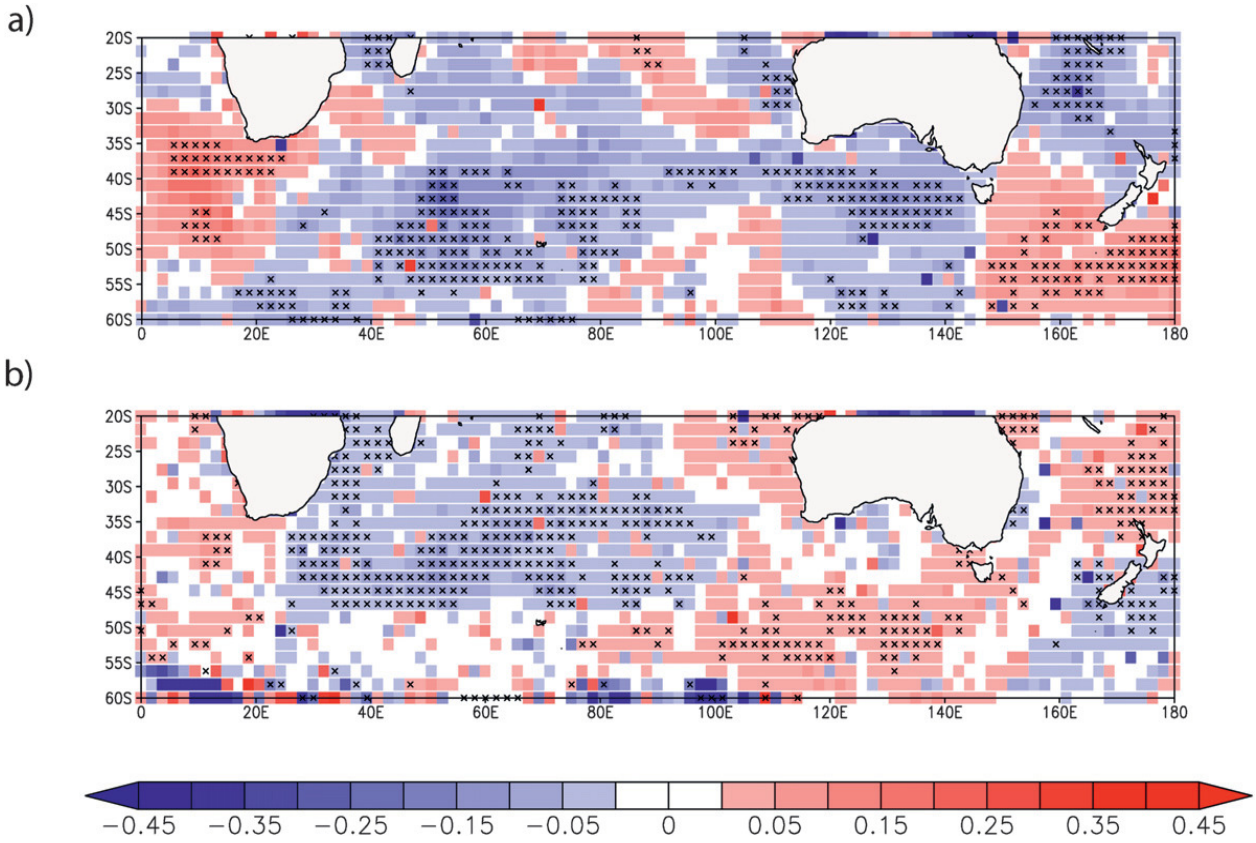

Figure 1: Average sea temperature anomalies (^{o}C) over the ocean for the seven days before a CE in (a) Melbourne summer and (b) Perth winter. Areas marked with a cross indicate regions of where the anomalies differ significantly from zero at the 90% confidence level.

Atlantic hurricanes and European weather

Glebova E.S., Pokhil A.E.
Hydrometeorological Centre of Russia
ek.glebova@gmail.com

Tropical cyclones play a great role in the general circulation of atmosphere as they transfer large amounts of energy from tropical zone towards high latitudes. Interaction between tropical cyclones and the polar front accompanied by the release of energy accumulated by the vortex is often observed.

A case study concerning influence of an Atlantic hurricane on European weather is discussed in this paper. It is demonstrated that positive temperature anomalies in Europe in November 2008 were partly due to hurricane "Omar" which had been developing over the Atlantic ocean from the 13th to the 18th of October. The numerical ETA model of the atmosphere was used to predict trajectories and meteorological fields' dynamics in "Omar".

Tropical cyclone "Omar" originated from a tropical wave in the south-east of the Caribbean sea on the 13th of October 2008 and began moving northeastward. Its trajectory lay across the Central Atlantic. On the 15th of October "Omar" was given a status of a hurricane while the largest intensity of the vortex was registered on the 16.10 during its passage over Virginian Islands. On the 17.10 "Omar" had already possessed typical structure of a hurricane: the cloudless and windless eye of the storm in the centre and the circle of storm winds surrounding it. The wind speed reached 22 m/s at 10 meters and 25-30 m/s at 850 hPa. Kinetic energy maximum at almost all altitudes corresponded the area of the highest velocity values (Pic.1a). At the upper level of the boundary layer the kinetic energy maxima occupied the whole zone of "Omar" and an extra-tropical perturbation developing to the north of the hurricane (Рис.1 d). Vortices were not observed in the upper troposphere, a strong meridional flow (with wind speeds up to 30-50 m/s) possessing high values of kinetic energy corresponded these areas.

At 12 GMT on the 17.10 "Omar" started interacting with the polar front approaching low latitudes and the extra-tropical synoptic-scale disturbance mentioned earlier in the paper. Modification of the velocity field occurred. A strong southern flow uniting two cyclones appeared in the lower and in the middle troposphere. Their interaction expressed in consolidation of vorticity and kinetic energy maxima zones became apparent at 850 hPa (Pic. 1d,e,f).

The absolute values of kinetic energy of the extra-tropical cyclone exceeded these in "Omar". Besides that, the polar-frontal cyclone began to deepen rapidly. The reinforcement of environmental flow happened at 250 hPa.

Both vortices were situated on the western periphery of North-Atlantic maximum and were propagating northeastward. The extra-tropical cyclone possessed a well-developed warm sector with a tropical maritime air mass circulating in it (Pic. 1g), while the cold polar and arctic air was penetrating behind the cold front. Both cyclones were rather small and weak, so they could not spread towards the upper troposphere. At the altitude of 1.5 km one could observe both cyclones, however, tropical cyclone "Omar" was expressed better (Pic. 1c)

Calculations made for 18 GNT 17.10 showed two separated fronts of the extra-tropical cyclone that had turned from a wave into a young cyclone (Pic.1e,f). An extensive common belt of vorticity joining two cyclones formed at 850 hPa (Pic.1e), it can serve as an indicator of interaction between the tropical cyclone and the polar front. In the end of the 17.10 a sufficient thermal heterogeneity appeared in "Omar" which was accompanied by the rapid deepening of the extra-tropical cyclone moving northeastward (Pic.1g).

The interaction of vortices continued during the 18.10. The south-western stream formed by the cyclones brought warm and very humid air in the northern regions of the Atlantic. On the 19.10 "Omar", being involved into the strong flow, began moving northeastward to European shore and got into the baric trough of the extra-tropical cyclone, which led to the merging of the cyclones. The polar front was clearly identified in the vorticity field and this powerful formation influenced considerably the weather in Europe.

So we can conclude that computational results produced by ETA model demonstrated that tropical cyclone "Omar" interacted with the polar front and the synoptic disturbance developing on it; the interaction of these structures led to the energy transfer from "Omar" to the extra-tropical cyclone and to the intensification of the latest. The large amounts of energy accumulated by the hurricane played a considerable role in the formation of positive temperature anomalies in autumn of 2008 in Europe.

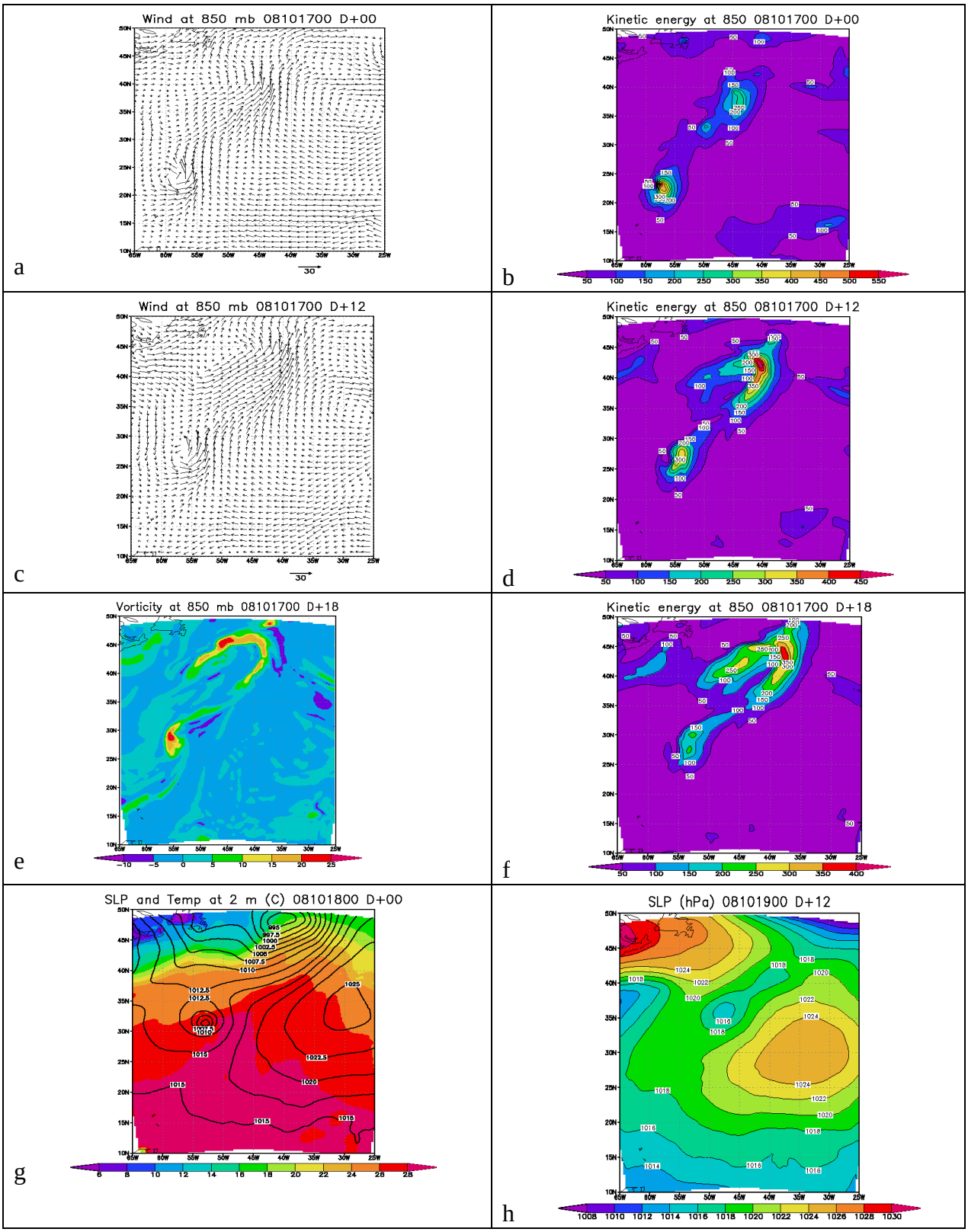

Pic.1. a) Wind at 850 hPa 17.10.2008 0 GMT; b) Kinetic energy at 850 hPa 17.10.2008 0 GMT; c) Wind at 850 hPa 17.10.2008 12 GMT; d) Kinetic energy at 850 hPa 17.10.2008 12 GMT; e) Vorticity at 850 hPa 17.10.2008 18 GMT; f) Kinetic energy at 850 hPa 17.10.2008 18 GMT; g) Sea-level pressure and temperature at 2 meters 18.10.2008 0 GMT; h) Sea-level pressure and temperature at 2 meters 19.10.2008 12 GMT

On analysis of typhoon activities from a thermodynamic viewpoint

Shinya Shimokawa * and Hisashi Ozawa **

* National Research Institute for Earth Science and Disaster Prevention, Tsukuba, Japan
** Hiroshima University, Higashi-Hiroshima, Japan

1. Introduction

Typhoons form in the region where sea surface temperature is high, usually at about 27 degrees Celsius. A typhoon moves from the formation region. The forecast of the track is difficult even when using high-resolution numerical models. It, however, will be certain that a typhoon decays gradually when it moves over a region with low temperature and the energy supplied from the region is small. Thus, the ratio of the number of tropical cyclones which land on Japan with typhoon intensity to that of all tropical cyclones which approach Japan will be high when sea surface temperature around Japan is high.

Strictly speaking, the formation and track of typhoons are related to not only sea surface temperature but also vertical structure of the atmosphere and sea level pressure because when considering typhoon as a heat engine, the high-temperature reservoir is at the sea surface and the low-temperature reservoir is at the tropopause. Thus, it is desirable to use an index reflecting these factors when considering the formation and track of typhoons. Maximum potential intensity (MPI: Emanual, 1987) is known as one of such indices.

It is considered from a dynamic viewpoint that typhoons are carried by a synoptic-scale wind system which includes typhoons themselves. Especially for typhoons which land on Japan, the position of North Pacific high-pressure for 500-700 hPa is considered to be important. Our thermodynamic viewpoint does not contradict the above view, but gives a different viewpoint, e.g. an important suggestion for typhoon activities in the cases with difficulties in the forecast of exact dynamic fields such as simulations for global warming.

On the basis of the above idea, we investigate the relationship between MPI (calculated from NCEP reanalysis 2 and NOAA OISST V2) and typhoon tracks (RSMC Tokyo best track data) during 1982-2005.

2. Method of Analysis and Data

Let us consider the following index:

Index = (MPI at the location of a typhoon)
/ (longitudally averaged MPI over the latitude including the typhoon)

The index is averaged over the path of the typhoon. The index larger than 1.0 means that the typhoon moves across regions with relatively large MPI. The index smaller than 1.0 means that the typhoon moves across regions with

relatively small MPI.

In this study, minimum potential pressure is used as MPI. Therefore, the index should be smaller than 1.0 when the typhoon moves across regions with relatively large MPI. The index should be larger than 1.0 when the typhoon moves across regions with relatively small MPI. The index should be nearly 1.0 when the path of the typhoon is irrelevant to MPI.

Information about data used in this study is as follows:
Data for calculation of MPI: NCEP 2 and NOAA OISST V2 (monthly mean)
Data for typhoon path: RSMC Tokyo best track data
Period: 1982-2005
Region: 125E-185E (123.75E-186.25E), 2.5N-30N (1.25N-31.25N)
Interpolation: time and longitude

3. Results

Results for the calculated index are summarized as follows;

Averages: 0.9958 (averaged over all typhoons), 0.9669 (averaged over all data points). The number of typhoons is 633, and the number of data points for typhoon paths is 23991. In all typhoons moving across the region (554 typhoons), the number of typhoons with the indices smaller than 1.0 is 462 (83%). In all data points within the region (13064 data points), the number of data points with the indices smaller than 1.0 is 8802 (67%).

Latitudal change: In all latitudes (12 ranges from 2.5N to 30N with an interval of 2.5 deg.), the number of ranges with the indices smaller than 1.0 is 10 (83%). The ranges with the indices larger than 1.0 are 22.5N and 25.0N. The ranges with the indices of nearly 1.0 are 5.0N and 7.5N.

Annual change: In all years (24 years), the number of years with the indices smaller than 1.0 is 21 (88%). The years when a ratio of the number of typhoons with the indices smaller than 1.0 to the total number of typhoons is relatively low are 1984, 1985, 1996, 1997, 2000. There exist large annual variations. In 1982, 1983, 1989, 1998, 1999, and 2003, all typhoons have the indices smaller than 1.0 (the ratios are 1.0). In contrast, the ratios are 209/449 (46%) in 1984, 192/472 (40%) in 1985, 174/621 (28%) in 1996, 305/828 (37%) in 1997, and 84/451 (17%) in 2000.

Monthly change: In all months with data (213 months), the number of months with the indices smaller than 1.0 is 160 (75%). The month with the index larger than 1.0 is only February. The months with the indices of nearly 1.0 are September and October. The months with the indices not very smaller than 1.0 are February, March, September, and October. Note that the denominator in the ratio (the number of typhoons) is relatively small in February.

More detailed discussions will be presented in future publications.

References:

K. Emanuel 1987, Nature, 326, 483-485

Fall Arctic synoptic changes and sea ice reductions

Ian Simmonds and Kevin Keay

School of Earth Sciences, The University of Melbourne, Victoria, 3010, Australia
simmonds@unimelb.edu.au

Many aspects of changes in Arctic climate have been documented recently (Stroeve et al. 2007, Simmonds et al. 2008). Synoptic activity and sea ice coverage interact in numerous complex ways, so it is logical to explore the extent to which recent changes in Arctic storm activity and in sea ice coverage are linked. We identified all September Arctic MSLP cyclones over the period 1979-2008 using the JRA-25 global reanalysis (Onogi et al. 2007). For this we used The University of Melbourne cyclone tracking scheme (Simmonds et al. 2003), which diagnoses many key features of cyclone structure, including Depth and Radius. The Sea Ice Extent (SIE) data was sourced from NSIDC.

The greatly reduced September Arctic sea ice coverage in recent years is shown in Fig. 1. The time series of September Arctic SIE is presented in the top panel of Fig. 2. It exhibits a significant decline over the last three decades ($p < 0.001$) of 0.728×10^6 km^2 decade^{-1}. Noteworthy variations in September synoptic activity have also occurred in the Arctic basin over the period. The mean number of cyclone displays no significant trend (Fig. 2b). By contrast there are strong and significant positive trends in mean cyclone Depth (1.58 hPa century^{-1}, $p = 0.037$) and Radius (0.70 ^{o}latitude century^{-1}, $p = 0.001$) (parts c, d), and the last few years have witnessed extreme values of these cyclone characteristics. These basin-wide trends hint at links between SIE and cyclone vigour rather than frequency. The other panels in Fig. 2 show the variability of other key climate indicators. Of especial interest is the latent heat flux which has shown a significant upward trend (7.02 Wm^{-2} century^{-1}, $p = 0.066$), and has displayed large values since 2002, representing a potential increase in energy available to cyclones.

Fig. 2 suggests that years of low September Arctic SIE are associated with stronger and larger cyclones. We quantify this by correlating the raw time series of SIE with those of the cyclone properties displayed in Fig. 2. The mean September Depth is correlated with SIE with a coefficient (r) of -0.52 ($p = 0.003$), while $r = -0.65$ ($p = 0.001$) for the monthly mean Radius. (There is no significant correlation between SIE and cyclone frequency.) There is also a significant, albeit smaller, negative association between the SIE and the latent heat flux of -0.37 ($p = 0.046$).

The findings, discussed more fully in Simmonds and Keay (2009), reinforce suggestions that the decline in the extent and thickness of Arctic ice has started to render it particularly vulnerable to future anomalous cyclonic activity and atmospheric forcing.

Onogi, K., and Coauthors, 2007: The JRA-25 reanalysis. *J. Meteor. Soc. Japan,* **85,** 369-432.

Simmonds, I., and K. Keay, 2009: Extraordinary September Arctic sea ice reductions and their relationships with storm behavior over 1979-2008. *Geophys. Res. Lett.,* **39,** L19715, doi:10.1029/2009GL039810.

Simmonds, I., and Coauthors, 2003: Synoptic activity in the seas around Antarctica. *Mon. Wea. Rev.,* **131,** 272-288.

Simmonds, I., and Coauthors, 2008: Arctic climate change as manifest in cyclone behavior. *J. Climate,* **21,** 5777-5796.

Stroeve, J., and Coauthors, 2007: Arctic sea ice decline: Faster than forecast. *Geophys. Res. Lett.,* **34,** L09501, doi:10.1029/2007GL029703.

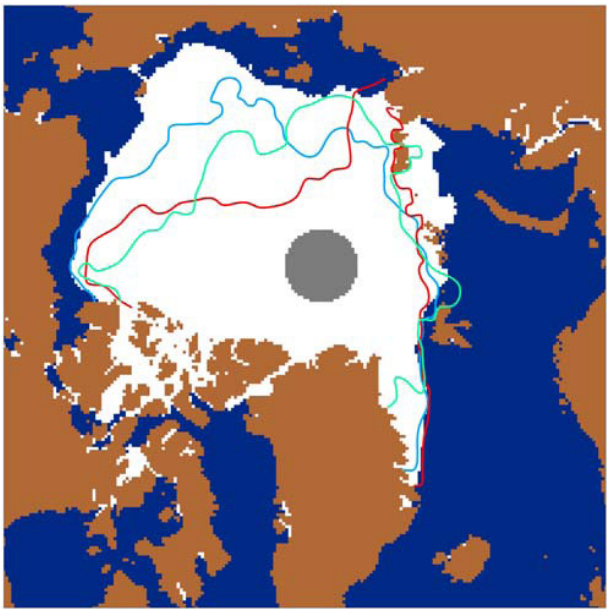

Figure 1: September Arctic sea ice coverage. The median ice cover (for 1979–2000) is presented in solid white. The blue, green, and red lines indicate the ice edges in 2005, 2008, and 2007, respectively.

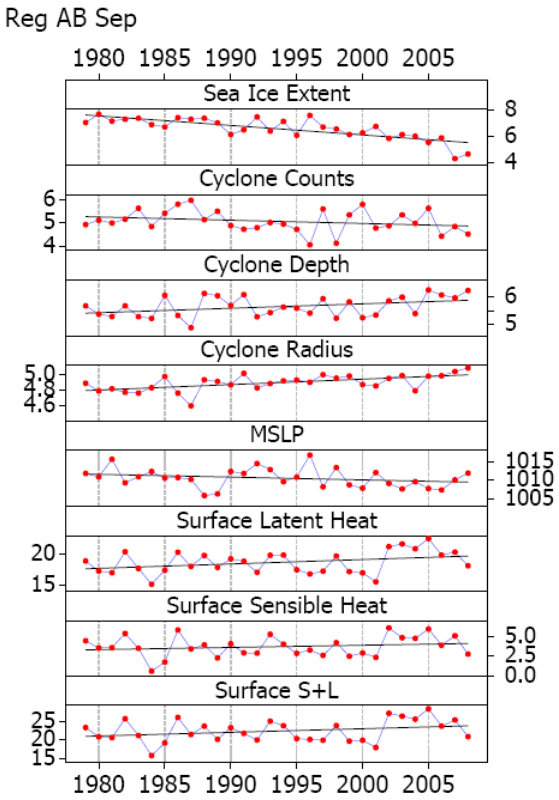

Figure 2: September Arctic basin mean time series 1979-2008. (a) Sea ice extent (in 10^6 km^2), (b) cyclone counts per analysis, (c) cyclone Depth (hPa), (d) cyclone Radius (^{o}latitude), (e) MSLP (hPa), (f) surface latent heat flux (Wm^{-2}), (g) surface sensible heat flux (Wm^{-2}), and (h) the sum of the last two (Wm^{-2}). The solid lines denote the line of best fit (least squares).

Recent southern Semiannual Oscillation fluctuations in ERA-Interim

Ian Simmonds and Rachel Badlan

School of Earth Sciences, The University of Melbourne, Victoria, 3010, Australia
simmonds@unimelb.edu.au

The existence of a semiannual oscillation (SAO) in the southern extratropics pressure has been known for many years (van Loon 1967). It results from the different thermal inertias in the sea ice-Antarctic region and the Southern Ocean. This results in a semiannual variation in the meridional temperature gradient and the effects on the baroclinicity are also modulated by the seasonality of the vertical stability (Walland and Simmonds 1999). The magnitude of the SAO has been shown to undergo considerable interannual and decadal fluctuations, it being particularly strong in the mid 1970s and then progressively weakened up to about 1990 (Simmonds and Jones 1998 (SJ)). The behaviour of the SAO strongly influences sea ice-atmosphere interactions (Simmonds and King 2004, Yuan and Li 2008).

We have examined the recent behaviour of the SAO using the ERA-Interim reanalysis (1989-2008). We calculated (using the methods of SJ) the amplitude of the second harmonic of the zonally-averaged MSLP calculated from the three-year running means. Fig. 1 shows the time-latitude plot of the amplitude of this mode. It will be seen that the amplitude remained high for most of the 1990s, and then weakened for a few years about the turn of the century. About 2004 it regained its customary strength of about 2 hPa.

While MSLP is a valuable index of atmospheric behaviour its physical meaning over regions of significant topography (such as over the high southern latitudes) can be limited. In particular, any annual modes in the near-surface temperature used to extrapolate the surface pressure (SP) to MSLP could distort the MSLP SAO signal. For this reason it is also of value to undertaken the above analysis using SP, the time-latitude behaviour being shown in Fig.2. As would be expected, the plot is similar to Fig. 1, except to the south of 70^{o}S where the role of topography become significant. The amplitude of SP SAO exceeds 3 hPa over the continent for the majority of the time, whereas that in the MSLP is considerably weaker.

The nature of the temporal SAO variability we observe in this updated analysis is consistent with that revealed in unforced and sensitivity experiments (e.g., boundary forcing) with climate models (Simmonds and Walland 1998, Walland and Simmonds 1998).

Simmonds, I., and D. A. Jones, 1998: The mean structure and temporal variability of the semiannual oscillation in the southern extratropics. *Int. J. Climatol.,* **18,** 473-504.

Simmonds, I., and D. J. Walland, 1998: Decadal and centennial variability of the southern Semiannual Oscillation simulated in the GFDL coupled GCM. *Climate Dyn.,* **14,** 45-53.

Simmonds, I., and J. C. King, 2004: Global and hemispheric climate variations affecting the Southern Ocean. *Antarc. Sci.,* **16,** 401-413.

van Loon, H., 1967: The half-yearly oscillations in middle and high southern latitudes and the coreless winter. *J. Atmos. Sci.,* **24,** 472-486.

Walland, D., and I. Simmonds, 1999: Baroclinicity, meridional temperature gradients, and the southern Semiannual Oscillation. *J. Climate,* **12,** 3376-3382.

Walland, D. J., and I. H. Simmonds, 1998: Sensitivity of the Southern Hemisphere semiannual oscillation in surface pressure to changes in surface boundary conditions. *Tellus,* **50A,** 424-441.

Yuan, X., and C. Li, 2008: Climate modes in southern high latitudes and their impacts on Antarctic sea ice. *J. Geophys. Res.,* **113,** C06S91, doi:10.1029/2006JC004067.

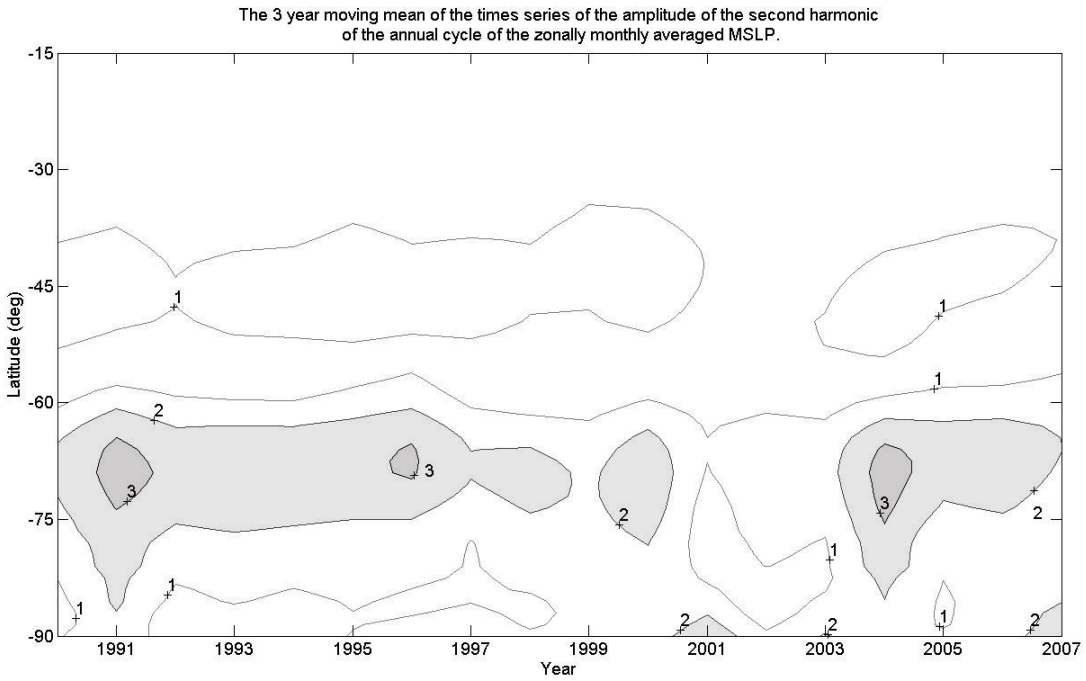

Figure 1: Time-latitude plot of the amplitude (hPa) of the semiannual oscillation in zonally-averaged MSLP in the ERA-Interim reanalysis. The semiannual mode is calculated from the mean annual cycle calculated over three consecutive years, and the amplitude plotted at the middle of those years.

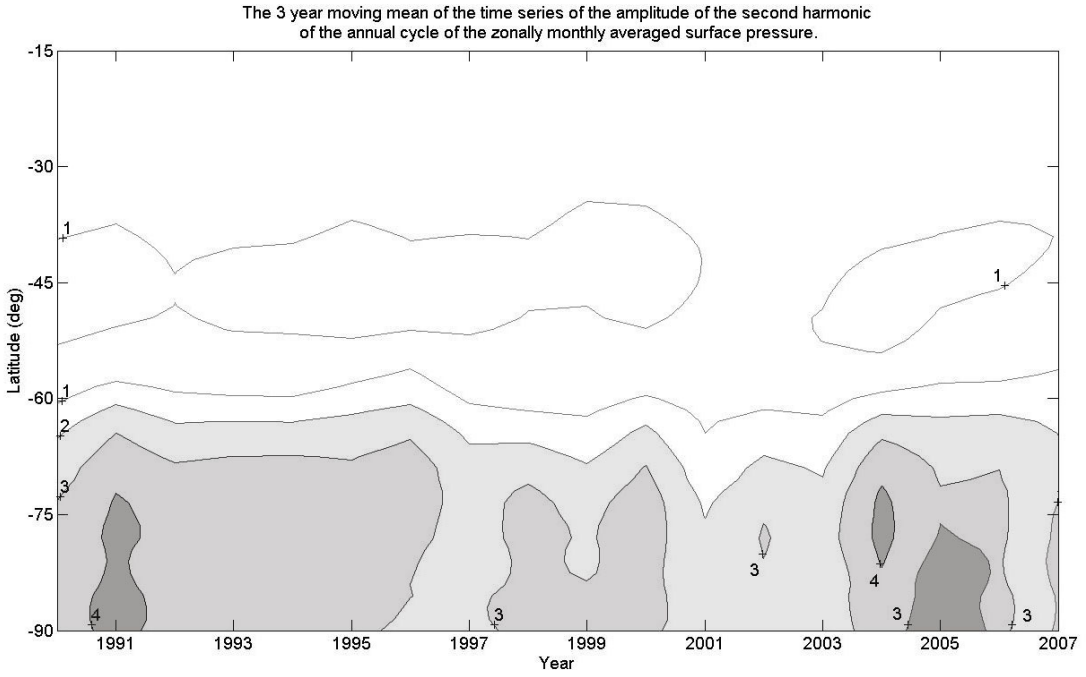

Figure 2: Time-latitude plot of the amplitude (hPa) of the semiannual oscillation in zonally-averaged SP in the ERA-Interim reanalysis. The semiannual mode is calculated from the mean annual cycle calculated over three consecutive years, and the amplitude plotted at the middle of those years.

Effect of temporal covariances on the apparent mean Eady growth rate

Ian Simmonds* and Eun-Pa Lim**

*School of Earth Sciences, The University of Melbourne, Victoria, 3010, Australia
simmonds@unimelb.edu.au
**Centre for Australian Weather and Climate Research, GPO Box 1289K Melbourne, Victoria, 3001, Australia

One of the simplest measures of baroclinicity was derived by Eady (1949). It pertains to the growth rate of the most unstable mode, and can be written as

$$\sigma = 0.3098 \frac{|f| \left| \frac{\partial U(z)}{\partial z} \right|}{N}$$

where N is the Brunt-Väisälä frequency ($N^2 = \frac{g}{\theta} \frac{\partial \theta}{\partial z}$, g being the acceleration due to gravity, z the vertical coordinate and θ the potential temperature) and f the Coriolis parameter, whose meridional derivative is denoted by β. $U(z)$ denotes the vertical profile of the background zonal velocity. In very many studies the time mean Eady growth rate is calculated from the means of the shear and of the Brunt-Väisälä frequency (method M). However, the growth rate expression is a nonlinear combination of these two variables and hence, in general, this is not an appropriate technique to calculate the mean growth rates. It can be argued that a more appropriate method to calculate the time mean growth rates at a given location is to calculate the rates at each synoptic time over a given epoch, and then take the average of those rates. This approach takes into account the temporal covariances associated with transient systems (method T).

We investigate the effect of these temporal covariances on the apparent mean Eady growth rate with the Japanese 25-year reanalysis (JRA-25) (Onogi et al. 2007). The reanalysis data set is archived every 6 hours and is available on a global 2.5° x 2.5° lat.-long. grid. We use the data for period of 1979–2007. The top panel in Fig. 1 shows the mean SH winter (JJA) 500 hPa growth rate calculated using the 'classical' method (method M). By contrast, the middle panel displays the rates when synoptic information is used (method T). The difference (T minus M) is shown in the bottom panel, and it shows that in the midlatitudes the significant changes are confined to the Pacific sector (particularly in the lee of Tasmania and New Zealand). Method T diagnoses increasingly greater growth rates with latitude which culminate in differences in excess of 0.15 day^{-1} off much of Antarctica. These represent large changes to the diagnosed baroclinicity around and to the south of 60°S, and are consistent with the high observed rates of cyclogenesis at these high latitudes (Simmonds et al. 2003).

The structure of the difference plot indicates that the application of Method T shifts the zones of maximum baroclinicity to the south. Our experiments indicate that care must been taken when calculating and interpreting simple measures of baroclinicity. Further details may be found in Simmonds and Lim (2009).

Eady, E. T., 1949: Long waves and cyclone waves. *Tellus,* **1,** 33-52.
Onogi, K., and Coauthors, 2007: The JRA-25 reanalysis. *J. Meteor. Soc. Japan,* **85,** 369-432.
Simmonds, I., and E.-P. Lim, 2009: Biases in the calculation of Southern Hemisphere mean baroclinic eddy growth rate. *Geophys. Res. Let.,* **36,** L01707, doi:10.1029/2008GL036320.
Simmonds, I., and Coauthors, 2003: Synoptic activity in the seas around Antarctica. *Mon. Wea. Rev.,* **131,** 272-288.

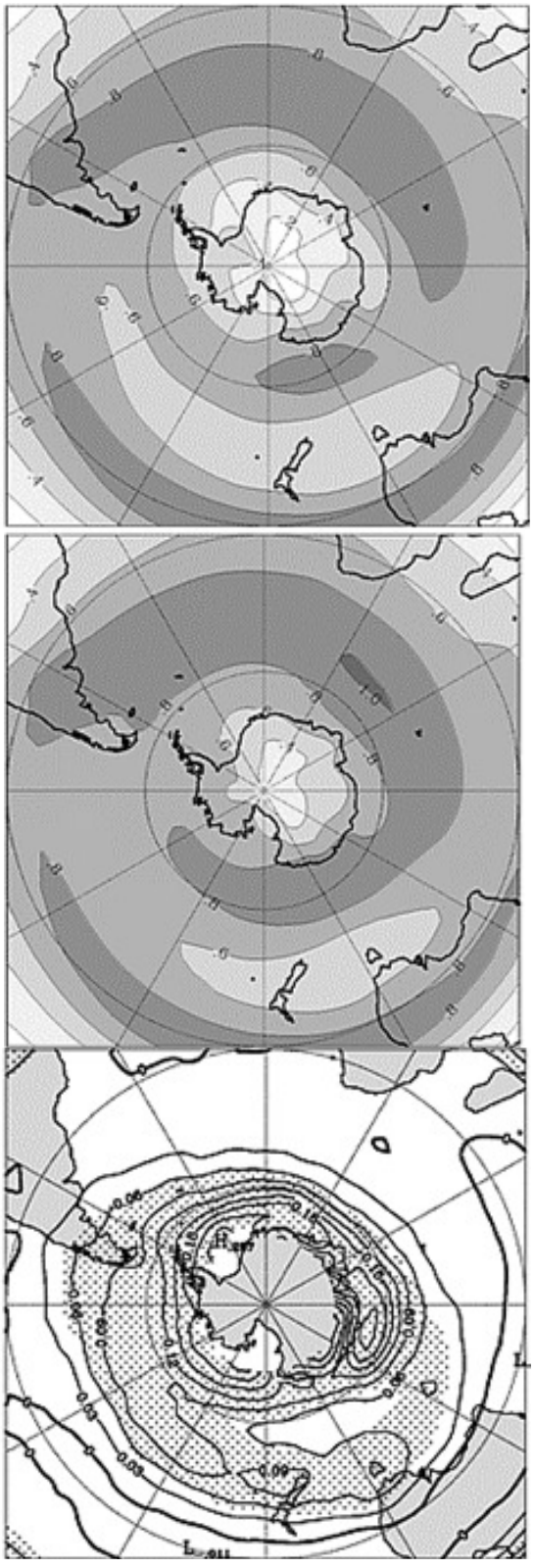

Figure 1: Climatology of the JJA maximum Eady growth rate at 500 hPa calculated with (top) seasonal mean vertical shear and *N* (method M) and (middle) 6-hourly vertical shear and *N* (method T). The bottom panel shows the difference (T minus M). The contour interval is 0.2 day^{-1} in the top two panels, and 0.03 day^{-1} in the bottom panel. The stippled area in this last indicates that the difference is significantly different from zero at the 95% confidence level (data poleward of 75°S are masked).